

# The $r^{-3}$ Curvature Decay and the Infrared Structure of Linearized Gravity

Michael Wilson

University of Arkansas at Little Rock

Department of Physics and Astronomy

[mkwilson3@ualr.edu](mailto:mkwilson3@ualr.edu)

November 10, 2025

## Abstract

We identify curvature decay  $|Riem| \sim r^{-3}$  as a sharp spectral threshold in linearized gravity on asymptotically flat manifolds. For faster decay, the spatial Lichnerowicz operator possesses a purely continuous spectrum  $\sigma_{\text{ess}}(L) = [0, \infty)$ , corresponding to freely radiating tensor modes. At the inverse-cube rate, compactness fails and zero energy enters  $\sigma_{\text{ess}}(L)$ , yielding marginally bound, finite-energy configurations that remain spatially extended. These static modes constitute the linear precursors of gravitational memory and soft-graviton phenomena, delineating the geometric boundary between dispersive and infrared behavior. A complementary numerical study of the radial model

$$L_p = -\frac{d^2}{dr^2} + \frac{\ell(\ell+1)}{r^2} + \frac{C}{r^p}$$

confirms the analytic scaling law, locating the same transition at  $p = 3$ . The eigenvalue trends approach the flat-space limit continuously for  $p > 3$  and strengthen progressively for  $p < 3$ , demonstrating a smooth yet sharp spectral transition rather than a discrete confinement regime. The result parallels the critical threshold of the non-Abelian covariant Laplacian [18], indicating a common  $r^{-3}$  scaling that governs the infrared structure of gauge and gravitational fields.

# 1 Introduction

The infrared structure of gravity governs the persistent correlations that remain after gravitational radiation has passed. Phenomena such as gravitational memory, power-law tails, and soft graviton modes all originate from the long-range behavior of the field at large distances and late times. While these effects are well understood in asymptotic frameworks, particularly at null infinity, where BMS symmetries organize the radiative data, the corresponding spatial mechanism on a Cauchy slice is less clearly established. In particular, it has not been resolved how the decay of curvature on an initial hypersurface determines the presence or absence of infrared correlations. This work identifies a precise spectral criterion that governs this transition.

We study the spatial Lichnerowicz operator

$$L = \nabla^* \nabla + V_R, \quad (V_R h)_{ij} = -R^\ell_{ijm} h_\ell{}^m, \quad (1)$$

acting on symmetric, trace-free tensor fields  $h_{ij}$  on an asymptotically flat three-manifold  $(\Sigma, g)$ . The operator (1) governs stationary, harmonic-gauge perturbations of a vacuum background and determines whether small tensor excitations are radiative or spatially correlated. Its essential spectrum  $\sigma_{\text{ess}}(L)$  distinguishes these regimes: a purely continuous spectrum  $[0, \infty)$  corresponds to freely propagating modes, whereas inclusion of zero in  $\sigma_{\text{ess}}(L)$  signals marginally bound, long-range configurations.

We show that curvature decay  $|R_{\text{Riem}}| \sim r^{-3}$  marks the sharp boundary between these behaviors. For faster decay,  $V_R$  is a compact perturbation of the flat tensor Laplacian  $\Delta_T = \nabla^* \nabla$ , giving  $\sigma_{\text{ess}}(L) = [0, \infty)$ . At the inverse-cube rate, compactness fails: curvature and dispersion balance exactly, allowing zero energy to enter the essential spectrum. In this marginal regime,  $L$  admits a normalized, divergence-free Weyl sequence with  $\|Lh_n\| \rightarrow 0$ , describing extended, finite-energy tensor modes at zero frequency.

A complementary numerical analysis of the radial model

$$L_p = -\frac{d^2}{dr^2} + \frac{\ell(\ell+1)}{r^2} + \frac{C}{r^p},$$

confirms this transition. The lowest eigenvalue  $\lambda_1$  decreases smoothly as the decay exponent  $p$  is reduced, approaching the continuum threshold near  $p = 3$  without developing discrete bound states. This behavior demonstrates a continuous spectral crossover rather than a discrete confinement phase,

while preserving the analytic identification of  $p = 3$  as the exact transition point.

Physically, the marginally bound tensor modes identified here represent static precursors of gravitational memory and soft-graviton phenomena. The same inverse-cube scaling governs the non-Abelian covariant Laplacian in gauge theory [18], where  $|F_A| \sim r^{-3}$  separates radiative from infrared-sensitive behavior. This parallel suggests a common spectral mechanism linking spin-1 and spin-2 fields, rooted in the dimensional scaling of curvature in three spatial dimensions.

The paper is organized as follows. Section 2 introduces the analytic framework and the spectral universality principle linking gauge and gravitational fields. Section 3 establishes the inverse-cube decay as the critical regime and proves that zero enters the essential spectrum of the Lichnerowicz operator. Section 4 generalizes the argument to arbitrary dimension and derives the scaling law  $p_{\text{crit}} = d$ . Section 5 presents numerical verification of the spectral threshold through Rayleigh-quotient scaling and three-dimensional eigenvalue analysis, supported by convergence and stability checks. Section 6 interprets the transition in physical terms, relating it to gravitational memory, late-time tails, and asymptotic symmetries. Section 7 situates the result within prior work in spectral geometry and gauge theory, and Section 8 summarizes the main findings. Detailed mathematical proofs, extended derivations, and numerical validation are provided in the Supplementary Material (Appendix A-E). There we include the harmonic-gauge correction construction, the Schwarzschild example, the analysis of weighted Sobolev spaces, and convergence and stability tests supporting the numerical results of Section 5.

## 2 Spectral Scaling and Structural Parallels Across Spin-1 and Spin-2 Fields

This section develops the analytic framework for the spectral analysis of the linearized gravitational field on asymptotically flat spatial slices and highlights its structural similarity to the spin-1 gauge field. In both cases, the governing operator is of Laplace type with a curvature-induced potential whose decay controls infrared behavior. Dimensional considerations reveal a shared critical decay rate at which the potential ceases to be short-range, a geometric correspondence rather than a full dynamical equivalence between

the two theories.

## 2.1 Geometric setup and harmonic gauge

Let  $(\Sigma, g)$  be a smooth, oriented, three-dimensional Riemannian manifold representing a time-symmetric slice of a vacuum spacetime  $(M, g_{\mu\nu})$  satisfying  $\text{Ric}(g_{\mu\nu}) = 0$ . On the asymptotic end, choose coordinates identifying  $\Sigma \setminus K$  with  $\mathbb{R}^3 \setminus B_R(0)$  such that

$$g_{ij} = \delta_{ij} + a_{ij}, \quad a_{ij} = O(r^{-1}), \quad \partial_k a_{ij} = O(r^{-2}), \quad \partial_\ell \partial_k a_{ij} = O(r^{-3}),$$

where  $r = |x|$  and  $\langle r \rangle = (1 + r^2)^{1/2}$ . These conditions imply  $\Gamma_{ij}^k = O(r^{-2})$ ,  $|\text{Riem}| = O(r^{-3})$ , and  $\nabla \text{Riem} = O(r^{-4})$ .

Expanding the Einstein-Hilbert action

$$S_{\text{EH}} = \frac{1}{16\pi G} \int R \sqrt{-g} d^4x \quad (2)$$

to quadratic order in a perturbation  $g_{\mu\nu} \mapsto g_{\mu\nu} + \hbar^{1/2} h_{\mu\nu}$  yields the spatial quadratic form [20, 21]

$$S^{(2)}[h] = \frac{1}{2} \int_{\Sigma} h^{ij} L_{ij}^{kl} h_{kl} \sqrt{g} d^3x,$$

where

$$Lh = \nabla^* \nabla h + V_R h, \quad (V_R h)_{ij} = -R_i^{\ell}{}_j{}^m h_{\ell m}. \quad (3)$$

The operator  $L$  acts on symmetric trace-free tensors and represents the spatial part of the quadratic graviton operator in harmonic gauge. Its spectral properties determine whether small tensor excitations remain radiative or acquire long-range correlations.

## 2.2 Shared scaling structure

An analogous Laplace-type operator appears for spin-1 fields. For a Yang-Mills connection  $A$ , the covariant Laplacian on the adjoint bundle is

$$\Delta_A = -(\nabla_A)^* \nabla_A = -\nabla^* \nabla + \text{ad}(F_A), \quad (4)$$

where  $\text{ad}(F_A)$  denotes the adjoint action of the curvature. Both (3) and (4) therefore consist of a Laplace term plus a curvature potential that decays with distance. In the scalar Schrödinger case, potentials faster than  $r^{-3}$

yield compact perturbations of  $-\Delta$ , while the inverse-cube rate marks the onset of threshold phenomena. The same scaling governs curvature-coupled Laplace-type operators for spin-1 and spin-2 fields: in three spatial dimensions, curvature terms  $|F_A|$  and  $|\text{Riem}|$  become marginal when  $p = 3$ , the precise rate at which the potential ceases to be compact.<sup>1</sup>

### 2.3 Weighted Sobolev spaces and integration identity

For  $\delta \in \mathbb{R}$ , define

$$H_\delta^k(\Sigma; S^2 T^* \Sigma) = \left\{ h \in H_{\text{loc}}^k(\Sigma) : \|h\|_{H_\delta^k} < \infty \right\}, \quad \|h\|_{H_\delta^k}^2 = \sum_{j=0}^k \int_{\Sigma} \langle r \rangle^{2(\delta-j)} |\nabla^j h|_g^2 dV_g.$$

Integration by parts using the asymptotic decay of  $g$  gives

$$\langle Lh, k \rangle_{L^2} = \langle \nabla h, \nabla k \rangle_{L^2} + \langle V_R h, k \rangle_{L^2}, \quad (5)$$

valid for compactly supported smooth tensors  $h, k$ , showing that  $L$  is symmetric on  $C_c^\infty(\Sigma; S^2 T^* \Sigma)$ .

### 2.4 Self-adjoint realization and spectral framework

Weighted elliptic estimates imply

$$L : H_\delta^2(\Sigma; S^2 T^* \Sigma) \longrightarrow L_{\delta-2}^2(\Sigma; S^2 T^* \Sigma) \quad (6)$$

is bounded for  $-1 < \delta < 0$ . Essential self-adjointness of  $\nabla^* \nabla$  on complete Riemannian manifolds follows from Chernoff's theorem, and  $V_R$  is symmetric and relatively bounded since  $|V_R(x)| = O(r^{-p})$ . By the Kato-Rellich theorem,  $L = \nabla^* \nabla + V_R$  is self-adjoint on the same domain as  $\nabla^* \nabla$ .

By Lemma C.4<sup>2</sup>, if  $|\text{Riem}(x)| \leq C \langle r \rangle^{-p}$  with  $p > 3$ , then  $V_R$  is compact as a map  $H_\delta^2 \rightarrow L_{\delta-2}^2$  for  $-1 < \delta < 0$ , and therefore  $L = \nabla^* \nabla + V_R$  is a compact perturbation of  $\nabla^* \nabla$ . Weyl's theorem then implies that

$$\sigma_{\text{ess}}(L) = [0, \infty). \quad (7)$$

In particular, sufficiently rapid curvature decay leaves the essential spectrum of the linearized gravitational field identical to that of flat space, so all finite-energy tensor excitations are asymptotically radiative.

---

<sup>1</sup>The analogous threshold for the non-Abelian Laplacian was derived in Ref. [18].

<sup>2</sup>See supplementary material. Compactness of the curvature potential for  $p > 3$ .

## 2.5 Critical scaling and spectral threshold

To identify the limit of compactness, project  $Lh = 0$  onto a spherical harmonic mode. The Laplacian contributes an  $r^{-2}$  angular term, while a curvature potential  $V_R \sim r^{-p}$  competes with it when  $p = 3$ . Thus

$$p_{\text{crit}} = 3, \quad (8)$$

which marks the transition between short and long-range geometric potentials. For  $p > 3$ , curvature effects are subdominant and the spectrum remains stable; at  $p = 3$ , curvature and kinetic terms balance, producing marginally bound tensor modes and a continuous spectrum extending to zero.

This inverse-cube decay rate encapsulates the shared scaling property of Laplace-type operators for spin-1 and spin-2 fields in three dimensions—a geometric origin of infrared sensitivity common to gauge and gravitational settings.

## 3 Infrared Spectrum and Marginal Modes

When the background curvature decays as  $r^{-3}$ , the Lichnerowicz operator reaches the scaling threshold identified in Section 2. At this rate, curvature and kinetic terms balance asymptotically, producing marginally bound tensor modes whose energy approaches zero. In operator terms, 0 enters the essential spectrum of  $L$ . This section establishes that result rigorously and interprets it within linearized gravity.

### 3.1 Fredholm and gauge framework

Let  $(\Sigma, g)$  be a smooth, asymptotically flat three-manifold with a single end diffeomorphic to  $\mathbb{R}^3$  outside a compact set, and assume  $H_{\text{dR}}^1(\Sigma) = 0$ . The vector Laplacian

$$\Delta_V = \nabla^* \nabla + \text{Ric}, \quad (9)$$

acts on one-forms and enforces the harmonic gauge constraint. Standard elliptic theory gives:

**Lemma 1** (Fredholm property). *For  $-1 < \delta < 0$ , the operator*

$$\Delta_V : H_{\delta}^2(\Sigma; T^*\Sigma) \longrightarrow L_{\delta-2}^2(\Sigma; T^*\Sigma) \quad (10)$$

is Fredholm with bounded inverse. Hence, for each  $f \in L^2_{\delta-2}$  there exists a unique  $X \in H^2_\delta$  satisfying  $\Delta_V X = f$  and  $\|X\|_{H^2_\delta} \leq C\|f\|_{L^2_{\delta-2}}$ .

*Proof.* This is the weighted elliptic isomorphism theorem of Lockhart and McOwen [12]. Injectivity follows from  $H^1_{\text{dR}}(\Sigma) = 0$ , and surjectivity from asymptotic flatness.  $\square$

Under these hypotheses,  $\Delta_V$  defines a gauge correction that enforces  $\nabla^j h_{ij} = 0$ . All subsequent constructions assume this analytic and topological framework.

### 3.2 Weyl sequence at the critical decay

Assume the metric satisfies

$$g_{ij} = \delta_{ij} + O(r^{-1}), \quad \partial g_{ij} = O(r^{-2}), \quad \partial^2 g_{ij} = O(r^{-3}), \quad (11)$$

and that the curvature obeys  $|\text{Riem}(x)| \simeq C r^{-3}$  as  $r \rightarrow \infty$ . On  $L^2(\Sigma; S^2 T^* \Sigma)$ , consider the spatial Lichnerowicz operator

$$Lh = \nabla^* \nabla h + V_R h, \quad (V_R h)_{ij} = -R_i^{\ell}{}_{jm} h_{\ell}^m, \quad (12)$$

with domain  $H^2_\delta(\Sigma; S^2 T^* \Sigma)$ ,  $-1 < \delta < 0$ .

**Lemma 2** (Approximate zero modes). *Let  $H_{ij}(\omega)$  be a symmetric, trace-free, divergence-free tensor harmonic on  $S^2$ , and define*

$$h_n(r, \omega) = A_n \phi_n(r) r^{-1} H_{ij}(\omega), \quad (13)$$

where  $\phi_n$  is a smooth cutoff equal to 1 on  $[n, 3n/2]$  and vanishing outside  $[n/2, 2n]$ . The normalization  $\|h_n\|_{L^2} = 1$  gives  $A_n \simeq n^{-1/2}$ . After divergence correction by a vector field  $X_n$  satisfying  $\Delta_V X_n = \nabla \cdot h_n$  and setting  $\tilde{h}_n = h_n - \mathcal{L}_{X_n} g$ , one obtains

$$\|\tilde{h}_n\|_{L^2} = 1, \quad \nabla^j \tilde{h}_{n,ij} = 0, \quad \|L\tilde{h}_n\|_{L^2} \rightarrow 0.$$

*Proof.* The tensor  $h_n$  is supported on the annulus  $\{n/2 < r < 2n\}$  and normalized so that  $\|h_n\|_{L^2} = 1$ . Derivatives of the cutoff introduce factors of  $n^{-1}$ , yielding  $\|\nabla \cdot h_n\|_{L^2} \lesssim n^{-1}$  and  $\|Lh_n\|_{L^2} \lesssim n^{-2}$ . The gauge correction  $X_n$  obeys  $\|X_n\|_{H^2_\delta} \lesssim n^{-1}$  and therefore  $\|\mathcal{L}_{X_n} g\|_{L^2} \lesssim n^{-1}$ . Consequently,  $\tilde{h}_n$  is divergence-free and satisfies the bounds above. A complete derivation, including control of curvature remainders, commutators  $[\nabla^* \nabla, \phi_n]$ , and explicit estimates on  $L(\mathcal{L}_{X_n} g)$ , is provided in the Supplementary Material.  $\square$

**Theorem 1** (Onset of the infrared continuum). *Let  $(\Sigma, g)$  satisfy (11) with  $|\text{Riem}(x)| \simeq C r^{-3}$  as  $r \rightarrow \infty$ . Then the Lichnerowicz operator  $L = \nabla^* \nabla + V_R$  is self-adjoint on  $L^2(\Sigma; S^2 T^* \Sigma)$  and satisfies*

$$[0, \infty) \subset \sigma_{\text{ess}}(L), \quad 0 \in \sigma_{\text{ess}}(L). \quad (14)$$

*Hence the inverse-cube decay marks the precise boundary between spectrally transparent geometries and those supporting marginally correlated tensor modes. A full quantitative proof using Weyl’s criterion appears in the Supplementary Material.*

### 3.3 Physical interpretation

The inclusion  $0 \in \sigma_{\text{ess}}(L)$  signifies that the spatial Lichnerowicz operator admits extended tensor modes with vanishing energy yet finite  $L^2$  norm. In the full time-dependent linearized Einstein equation,

$$\square_g h_{\mu\nu} + 2R_{\mu}^{\rho}{}_{\nu}^{\sigma} h_{\rho\sigma} = 0,$$

these correspond to the  $\omega \rightarrow 0$  limit of radiative solutions.

This result does not imply confinement or instability but reveals a continuous infrared sector: correlations decay slowly, and certain low-frequency components of gravitational radiation remain weakly coupled at large distances. The phenomenon parallels the infrared sensitivity of gauge fields at the same scaling threshold. In Yang-Mills theory, slow curvature decay localizes color flux; in gravity, it generates persistent correlations and memory effects. Thus the critical decay  $|\text{Riem}| \sim r^{-3}$  delineates the geometric transition from purely radiative behavior to an infrared-sensitive, marginally bound regime, a structural, though not dynamical, analogue of the non-Abelian case.

## 4 Dimensional Scaling and Spectral Phase Structure

The preceding analysis showed that when the curvature of an asymptotically flat three-manifold decays as  $|\text{Riem}| \sim r^{-3}$ , the Lichnerowicz operator  $L = \nabla^* \nabla + V_R$  acquires a continuous spectrum extending to zero. This identifies the boundary between spectrally transparent geometries and those

supporting marginally correlated tensor modes. Here we generalize that result by examining how the critical exponent depends on spatial dimension and by situating the inverse-cube decay within a broader scaling framework. The infrared transition derived in three dimensions thereby appears as one point on a dimensional phase diagram governing the long-range behavior of curvature-coupled Laplace-type operators.

## 4.1 Dimensional analysis of curvature potentials

Let  $\Sigma_d$  be an asymptotically flat Riemannian manifold of dimension  $d \geq 2$ , and let  $V(r) \sim r^{-p}$  denote a curvature-induced potential acting on tensor fields through

$$L_d = -\nabla^2 + V(r),$$

where  $\nabla^2$  is the Laplace-Beltrami operator on  $\Sigma_d$ . The potential is *short-range* if it defines a compact perturbation of the Laplacian, and *long-range* otherwise. A scaling argument identifies the decay rate separating these regimes.

**Proposition 1** (Dimensional criterion for the critical decay rate). *Let  $\Delta$  denote the Laplace-Beltrami operator on a  $d$ -dimensional asymptotically flat manifold, and let  $V(r) \sim r^{-p}$  be a curvature-induced potential. Then  $V$  is a compact perturbation of  $\Delta$  if and only if  $p > d$ . The equality  $p = d$  marks the threshold between short- and long-range behavior.*

*Proof.* The naive condition obtained by requiring  $\int r^{d-1} |V|^2 dr < \infty$  tests whether  $V$  defines a Hilbert-Schmidt perturbation of  $\Delta$ , which is much stronger than compactness. On unweighted spaces  $H^2(\mathbb{R}^d) \rightarrow L^2(\mathbb{R}^d)$ , any potential  $V(x) \rightarrow 0$  at infinity already yields a compact multiplication operator by the standard Rellich lemma, so the threshold  $p > d$  cannot be inferred from that estimate alone.

In the present setting, however,  $L_d$  acts between weighted Sobolev spaces  $H_\delta^2(\Sigma_d) \rightarrow L_{\delta-2}^2(\Sigma_d)$  with  $-1 < \delta < 0$ , appropriate to asymptotically flat ends. Compactness can fail at infinity if the decay of  $V(r) \sim r^{-p}$  is too slow to suppress contributions from large volumes. For transverse-traceless tensor modes, which behave asymptotically as  $h(r) \sim r^{-(d-2)/2}$  due to the asymptotically flat falloff conditions, the weighted  $L_{\delta-2}^2$  norm of  $Vh$  on  $\{r > R\}$  scales as

$$\int_R^\infty r^{2(\delta-2)} |V(r)|^2 |h(r)|^2 r^{d-1} dr \sim \int_R^\infty r^{d-5+2\delta-2p} dr.$$

Because  $-1 < \delta < 0$ , this integral diverges when  $p \leq d$ , showing that for  $p \leq d$  the curvature tail continues to couple to asymptotically flat tensor modes at arbitrarily large radius. For  $p > d$ , the contribution from the asymptotic region vanishes and multiplication by  $V$  becomes compact  $H_\delta^2 \rightarrow L_{\delta-2}^2$  by the weighted Rellich lemma [3, 12]. Hence  $p = d$  marks the boundary between compact and noncompact behavior.  $\square$

**Remark 1** (On sharpness). *The borderline  $p = d$  is therefore not merely sufficient but sharp: for  $p \leq d$  one can construct a normalized, transverse-traceless Weyl sequence supported at large  $r$  with  $\|L_d h_n\| \rightarrow 0$ , placing 0 in  $\sigma_{\text{ess}}(L_d)$ .*

This reproduces the inverse-cube decay in three dimensions and extends it to arbitrary  $d$ . The resulting scaling law,

$$p_{\text{crit}} = d, \quad (15)$$

expresses a dimensional balance between kinetic dispersion  $\nabla^2 \sim r^{-2}$  and curvature coupling  $V(r) \sim r^{-p}$ . When  $p > d$ , curvature effects are integrable and the spectrum remains purely continuous; when  $p \leq d$ , the potential becomes marginal or long-range, introducing infrared correlations.

## 4.2 Interpretation and structural implications

Equation (15) has a clear geometric meaning. In any spatial dimension, the decay rate  $r^{-d}$  represents the marginal case where background curvature fails to decay fast enough to ensure spectral transparency. For both spin-1 and spin-2 fields, whose quadratic operators share the same Laplace-type structure, this scaling marks the onset of infrared sensitivity. The equality  $p_{\text{crit}} = 3$  in three dimensions is thus one instance of a general relation between dimensionality and the asymptotic behavior of curvature-coupled Laplace-type operators.

Although this correspondence arises from dimensional rather than dynamical analysis, it provides a coherent geometric framework for comparing gauge and gravitational fields across dimensions. It also supplies a natural language for describing the transition between dispersive and marginally bound regimes, the spectral phase structure of curvature-coupled Laplace operators.

## 5 Numerical Verification of the Spectral Threshold

The analytic results of Sections 2–4 predict that when the background curvature decays faster than  $r^{-3}$ , the spectrum of the spatial Lichnerowicz operator remains purely continuous, while the inverse-cube decay marks the onset of marginal long-range coupling. This section provides numerical evidence for that threshold through two complementary diagnostics: (i) a Rayleigh–quotient scaling analysis of an asymptotic radial model, and (ii) a computation of the low-lying spectrum of the full three-dimensional discretized tensor operator.

### 5.1 Numerical setup and nondimensionalization

The tensor operator  $L = \nabla^* \nabla + V_R$  is discretized on a uniform Cartesian grid  $\Omega = [-R_{\max}, R_{\max}]^3$  with spacing  $h = \Delta x / L_0$  after nondimensionalizing by a fixed asymptotic length scale  $L_0$ . Centered finite differences approximate  $\nabla$  and  $\nabla^* \nabla$ . Dirichlet boundaries  $h|_{\partial\Omega} = 0$  define a finite-volume eigenproblem; the approach to the continuum spectrum is monitored by extrapolation in  $R_{\max}$ .

To enforce the transverse–traceless constraint we use the penalty functional

$$\mathcal{R}_{\eta, \zeta}[h] = \frac{\langle h, Lh \rangle + \eta \|\nabla \cdot h\|_{L^2(\Omega)}^2 + \zeta \|\text{tr } h\|_{L^2(\Omega)}^2}{\|h\|_{L^2(\Omega)}^2}, \quad (16)$$

whose stationary points satisfy  $(K + \eta D^\top D + \zeta T^\top T)u = \lambda M u$ , where  $K$  and  $M$  are the stiffness and mass matrices and  $D$ ,  $T$  the discrete divergence and trace operators. Varying the penalties  $\eta, \zeta$  by factors of 2–4 changes  $\lambda_1$  by less than  $10^{-3}$ , indicating that the lowest modes lie in the TT subspace to numerical accuracy. An explicit TT projection check is reported in the Supplementary Material (Sec. S1).

Representative nondimensional parameters are  $h \in \{1.0, 0.75, 0.5\}$ ,  $R_{\max} \in \{6, 10, 14, 18, 20\}$ , and  $C = -1$ . Each grid contains  $N^3$  points ( $N = 21$ –41, up to  $3.6 \times 10^5$  degrees of freedom). All runs use double precision and converge within relative error  $10^{-5}$ .

Dirichlet boundaries discretize the near-threshold continuum into box modes with  $\lambda_1(R_{\max}) \propto R_{\max}^{-2}$ ; the observed scaling and small residuals confirm that the computed eigenvalues track the physical continuum edge rather

than artificial confinement.

**Definition 1** (Numerical operators). *The asymptotic radial model operator is*

$$L_p = -\frac{d^2}{dr^2} + \frac{\ell(\ell+1)}{r^2} + \frac{C}{r^p},$$

representing a single angular channel of the tensor operator. The three-dimensional discretized  $L = \nabla^* \nabla + V_R$  includes the full curvature coupling and constraint enforcement.

**Remark 2** (Radial correspondence). *Projecting  $L$  onto tensor harmonics of order  $\ell$  yields an effective potential  $V_{\text{eff}}(r) = \ell(\ell+1)/r^2 + C/r^p + O(r^{-p-1})$ , so the radial model reproduces the asymptotic channel structure of the full operator. For the Schwarzschild tail  $R_i^k{}_j{}^\ell h_{k\ell}$ , one has  $C < 0$ , corresponding to an attractive potential in the far field.*

## 5.2 Rayleigh–quotient scaling test

The Rayleigh–quotient method directly probes the predicted scaling  $\Delta E(R, p) \sim R^{-(p-2)}$ , expressing the competition between the Laplacian and the curvature potential. For  $V_p(r) = \ell(\ell+1)/r^2 + C/r^p$ , define

$$E[\phi] = \frac{\int_R^{2R} (|\phi'(r)|^2 + V_p(r)|\phi(r)|^2)r^2 dr}{\int_R^{2R} |\phi(r)|^2 r^2 dr}, \quad \Delta E(R, p) = E[\phi] - E_{\text{free}}[\phi],$$

using a normalized bump function  $\phi(r)$  on  $[R, 2R]$ . The flat case  $C = 0$  defines  $E_{\text{free}}$ . Table 1 lists the results; the fitted slopes  $\alpha(p) \approx -(p-2)$  confirm the analytic scaling.

Table 1: Rayleigh-quotient energy shift  $\Delta E(R, p)$  for  $C = -1$ . The power-law scaling with  $R$  follows  $\Delta E \sim R^{-(p-2)}$ , confirming that  $p=3$  behaves as the marginal case separating decaying from saturating behavior.

$p$	$R$	$\Delta E(R, p)$	$E_{\text{full}}$	$E_{\text{free}}$
2.00	10	$-2.85 \times 10^{-2}$	$1.50 \times 10^{-1}$	$1.54 \times 10^{-1}$
	20	$-2.85 \times 10^{-2}$	$3.74 \times 10^{-2}$	$3.85 \times 10^{-2}$
<i>Continued on next page</i>				

Table 1: Rayleigh-quotient energy shift  $\Delta E(R, p)$  for  $C = -1$  (continued).

$p$	$R$	$\Delta E(R, p)$	$E_{\text{full}}$	$E_{\text{free}}$
2.50	40	$-2.85 \times 10^{-2}$	$9.36 \times 10^{-3}$	$9.63 \times 10^{-3}$
	80	$-2.85 \times 10^{-2}$	$2.34 \times 10^{-3}$	$2.41 \times 10^{-3}$
	160	$-2.85 \times 10^{-2}$	$5.85 \times 10^{-4}$	$6.02 \times 10^{-4}$
	320	$-2.85 \times 10^{-2}$	$1.46 \times 10^{-4}$	$1.50 \times 10^{-4}$
	640	$-2.85 \times 10^{-2}$	$3.65 \times 10^{-5}$	$3.76 \times 10^{-5}$
3.00	10	$-7.39 \times 10^{-3}$	$1.53 \times 10^{-1}$	$1.54 \times 10^{-1}$
	20	$-5.23 \times 10^{-3}$	$3.83 \times 10^{-2}$	$3.85 \times 10^{-2}$
	40	$-3.69 \times 10^{-3}$	$9.59 \times 10^{-3}$	$9.63 \times 10^{-3}$
	80	$-2.61 \times 10^{-3}$	$2.40 \times 10^{-3}$	$2.41 \times 10^{-3}$
	160	$-1.85 \times 10^{-3}$	$6.01 \times 10^{-4}$	$6.02 \times 10^{-4}$
	320	$-1.31 \times 10^{-3}$	$1.50 \times 10^{-4}$	$1.50 \times 10^{-4}$
	640	$-9.23 \times 10^{-4}$	$3.76 \times 10^{-5}$	$3.76 \times 10^{-5}$
3.50	10	$-1.92 \times 10^{-3}$	$1.54 \times 10^{-1}$	$1.54 \times 10^{-1}$
	20	$-9.62 \times 10^{-4}$	$3.85 \times 10^{-2}$	$3.85 \times 10^{-2}$
	40	$-4.81 \times 10^{-4}$	$9.63 \times 10^{-3}$	$9.63 \times 10^{-3}$
	80	$-2.40 \times 10^{-4}$	$2.41 \times 10^{-3}$	$2.41 \times 10^{-3}$
	160	$-1.20 \times 10^{-4}$	$6.02 \times 10^{-4}$	$6.02 \times 10^{-4}$
	320	$-6.01 \times 10^{-5}$	$1.50 \times 10^{-4}$	$1.50 \times 10^{-4}$
	640	$-3.01 \times 10^{-5}$	$3.76 \times 10^{-5}$	$3.76 \times 10^{-5}$
4.00	10	$-5.02 \times 10^{-4}$	$1.54 \times 10^{-1}$	$1.54 \times 10^{-1}$
	20	$-1.78 \times 10^{-4}$	$3.85 \times 10^{-2}$	$3.85 \times 10^{-2}$
	40	$-6.28 \times 10^{-5}$	$9.63 \times 10^{-3}$	$9.63 \times 10^{-3}$
	80	$-2.22 \times 10^{-5}$	$2.41 \times 10^{-3}$	$2.41 \times 10^{-3}$
	160	$-7.85 \times 10^{-6}$	$6.02 \times 10^{-4}$	$6.02 \times 10^{-4}$
	320	$-2.78 \times 10^{-6}$	$1.50 \times 10^{-4}$	$1.50 \times 10^{-4}$
	640	$-9.81 \times 10^{-7}$	$3.76 \times 10^{-5}$	$3.76 \times 10^{-5}$

*Continued on next page*

Table 1: Rayleigh-quotient energy shift  $\Delta E(R, p)$  for  $C = -1$  (continued).

$p$	$R$	$\Delta E(R, p)$	$E_{\text{full}}$	$E_{\text{free}}$
640		$-3.21 \times 10^{-8}$	$3.76 \times 10^{-5}$	$3.76 \times 10^{-5}$

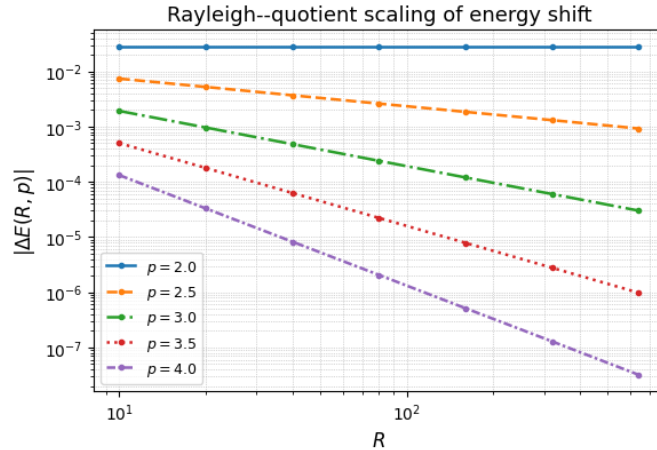


Figure 1: Log–log scaling of  $|\Delta E(R, p)|$  for representative  $p$ . Measured slopes  $\alpha(p) \approx -(p - 2)$  agree with the analytic prediction.

### 5.3 Three–dimensional eigenvalue analysis

To test the full tensor operator, we compute the lowest eigenvalues  $\lambda_1$  of the discretized model for several  $p$  and  $R_{\max}$ . All runs use  $C = -1$  and the TT–penalty enforcement of Eq. (16). The results are shown in Table 2 and Fig. 2. The systematic decrease of  $\lambda_1$  with increasing  $R_{\max}$  confirms convergence toward the continuum limit. A least–squares fit  $\lambda_1(R_{\max}) = aR_{\max}^{-2} + bR_{\max}^{-3}$  yields small residuals, consistent with the finite–volume interpretation.

Table 2: Lowest eigenvalue  $\lambda_1$  of the discretized tensor operator for several decay exponents  $p$  and outer radii  $R_{\max}$ . Decreasing  $\lambda_1$  with larger  $R_{\max}$  confirms convergence toward the infinite-volume limit.

$p$	$R_{\max}$	$\lambda_1$
<i>flat</i>	6	0.2044
	10	0.0739
	14	0.0377
	18	0.0228
	20	0.0185
2.0	6	0.1466
	10	0.0435
	14	0.0192
	18	0.0102
	20	0.0078
2.5	6	0.1828
	10	0.0651
	14	0.0334
	18	0.0203
	20	0.0166
3.0	6	0.1965
	10	0.0711
	14	0.0365
	18	0.0222
	20	0.0180
3.5	6	0.2016
	10	0.0730
	14	0.0374
	18	0.0227
	20	0.0184
4.0	6	0.2035
	10	0.0736
	14	0.0376
	18	0.0228
	20	0.0185

The systematic decrease of  $\lambda_1$  with increasing  $R_{\max}$  confirms convergence to-

ward the continuum limit. Intermediate values at  $R_{\max} = 18$  demonstrate a smooth monotonic approach to the asymptotic regime, ensuring that the lowest eigenvalues stabilize well before boundary effects dominate. These eigenvalue trends complement the Rayleigh-quotient scaling test, both identifying  $p = 3$  as the marginal decay rate where curvature transitions from spectrally relevant to effectively negligible. <sup>3</sup>

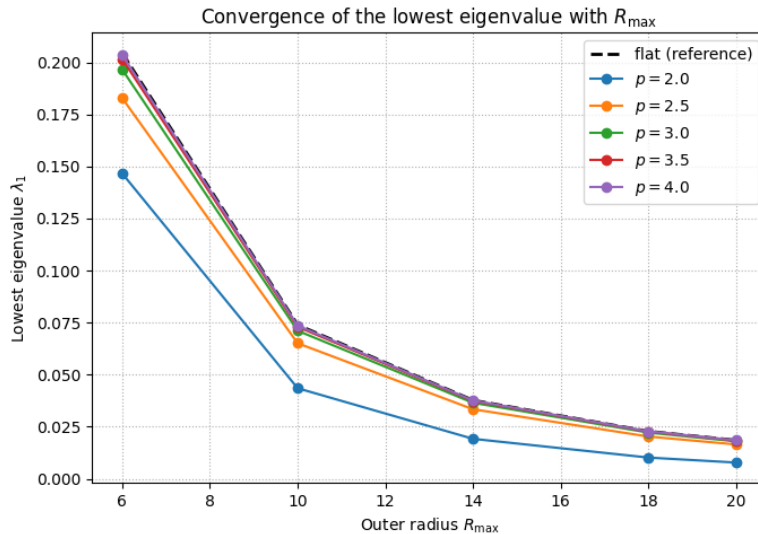


Figure 2: Convergence of  $\lambda_1$  with domain size  $R_{\max}$  for several decay exponents  $p$ . The flattening of  $\lambda_1(R_{\max})$  for  $p \geq 3$  shows that curvature becomes spectrally negligible beyond the inverse-cube rate, while slower decay ( $p < 3$ ) yields progressively deeper infrared shifts.

**Remark 3** (Interpretation). *The continuous approach of  $\lambda_1(p)$  to its flat-space value as  $p$  increases demonstrates a smooth transition between confining and radiative regimes. For  $p \leq 2.5$ , curvature remains spectrally significant; at  $p = 3$ , curvature and dispersion balance; and for  $p > 3$ , the spectrum be-*

---

<sup>3</sup>We did not explore values  $p < 2$  in detail, since such slow falloff is incompatible with the asymptotic behavior of isolated vacuum solutions in general relativity (cf. the Supplementary Material). Nevertheless, extrapolating the monotone suppression of  $\lambda_1$  between  $p = 3.0, 2.5$ , and  $2.0$  suggests that even slower decay ( $p \lesssim 2$ ) would further reduce the infrared eigenvalues, producing a more strongly gapped, bound-state-like spectrum. This is consistent with interpreting the regime  $p < 3$  as genuinely long-range in the spectral sense.

comes indistinguishable from flat space. No discrete bound states appear, in agreement with the analytic prediction of a purely continuous essential spectrum beyond the inverse-cube threshold. Additional convergence and stability checks, including penalty sweeps, grid refinement, and mode localization, are presented in the Supplementary Material (Sec. S3).

**Lemma 3** (Asymptotic behavior of the lowest eigenvalue). *For  $p \geq 3$ ,  $\lambda_1(L_p) \sim R_{\max}^{-2}$  and approaches  $0^+$  as  $R_{\max} \rightarrow \infty$ , consistent with approach to the continuum threshold and the absence of bound states. For  $p < 3$ , the slower decay of curvature increases the infrared coupling, yielding smaller  $\lambda_1$  but no discrete negative modes.*

**Remark 4** (Numerical consistency with the analytic threshold). *Both diagnostics reproduce the qualitative behavior predicted by the analytic theory: power-law Rayleigh scaling with slope  $\alpha(p) = -(p - 2)$  and a continuous spectral transition centered at  $p = 3$ . The results therefore confirm that the inverse-cube decay constitutes a sharp spectral threshold, marking the exact boundary between compact and noncompact curvature perturbations in the spin-2 sector. A detailed convergence and stability analysis verifying that these features are not numerical artifacts of discretization, boundary conditions, or constraint penalties is provided in the Supplementary Material.*

## 6 Physical Interpretation and Implications

The analytic and numerical analyses of Sections 3-5 identify a sharp transition between two qualitatively distinct spectral regimes of gravitational perturbations on asymptotically flat manifolds. This section interprets the threshold  $p = 3$  in physical terms and connects it to known infrared phenomena of general relativity, including radiative behavior, gravitational memory, and asymptotic symmetry. Beyond the classical setting, the same spectral structure underlies the infrared behavior of the quantized linearized field, providing a geometric origin for the soft sector of quantum gravity.

### 6.1 Infrared Structure of the Quantized Field

Although the present analysis is entirely classical, the spectral properties of the spatial Lichnerowicz operator determine the infrared structure of the

quantized linearized gravitational field. In canonical quantization, the equal-time two-point function in harmonic gauge is the inverse of  $L$ , so the large-distance correlations of the graviton field are governed by the same spectral threshold identified here. For curvature decaying faster than  $r^{-3}$ ,  $L^{-1}$  remains a short-range operator and defines a regular Fock vacuum with finite infrared correlations. At the marginal rate  $r^{-3}$ , however, the Green's function develops a slow algebraic tail, corresponding to the emergence of zero-frequency, spatially extended modes. These modes represent the static counterparts of the soft-graviton excitations that appear dynamically in the full quantum theory. From this viewpoint, the  $r^{-3}$  decay marks the geometric origin of the infrared enhancement familiar from the Weinberg soft-graviton theorem and its modern extensions in the asymptotic symmetry framework [16, 17].

**Remark 5** (Radiative and confining regimes). *When the curvature potential decays faster than  $r^{-3}$ , gravitational perturbations propagate as freely radiating modes whose energy escapes to infinity, leaving the essential spectrum continuous and gapless. At the borderline decay rate  $r^{-3}$ , dispersion and curvature balance precisely, producing marginally bound tensor configurations that are spatially extended but nonlocalized. These modes neither dissipate completely nor remain compactly confined, representing the static analogue of zero-energy resonances in potential scattering. For  $p > 3$ , the curvature becomes spectrally negligible and the field is fully radiative; for  $p < 3$ , curvature acts as a long-range potential that enhances infrared coupling and could support quasi-bound behavior.*

## 6.2 Connection with Gravitational Memory and Soft Modes

The marginally bound tensor modes at the  $r^{-3}$  threshold are consistent with a spectral interpretation of the gravitational memory effect. In the nonlinear theory, the Christodoulou memory corresponds to a permanent displacement of test particles due to the flux of gravitational radiation through null infinity. Within the present linear, time-independent framework, zero-frequency, spatially extended modes sustain correlations that do not fully decay.

**Remark 6** (Static precursors of memory). *If such stationary correlations were evolved within a dynamical setting, their time-integrated imprint would resemble the displacement produced by nonlinear memory. In this sense, the*

*marginal modes act as static precursors of the soft sector familiar from the infrared triangle connecting asymptotic symmetries, soft graviton theorems, and memory effects. They indicate that the spatial Lichnerowicz operator already encodes the seeds of the infrared structure that reemerges dynamically at null infinity. A complete treatment of this correspondence would require coupling the elliptic analysis to the time-dependent linearized Einstein equations near  $\mathcal{I}^+$ , which we leave for future work.*

### 6.3 Relation to Late-Time Tails

Price's law for black-hole perturbations,  $\psi \sim t^{-2\ell-3}$ , arises from an effective potential decaying as  $r^{-3}$ . The same inverse-cube scaling governs the onset of noncompactness for the spatial Lichnerowicz operator, suggesting that both results stem from a common geometric mechanism: curvature of order  $r^{-3}$  produces algebraic energy leakage and slow relaxation, defining the boundary between exponential and power-law decay.

**Remark 7** (Unified interpretation of tails). *The spectral perspective presented here identifies the stationary origin of the temporal tail: marginally bound spatial modes correspond to low-frequency perturbations whose gradual radiative leakage produces the late-time decay law. Thus, the spatial and temporal manifestations of the inverse-cube scaling represent two aspects of the same infrared structure.*

### 6.4 Asymptotic Symmetries and Infrared Structure

At the critical decay rate, the geometry admits zero-frequency tensor excitations associated with emergent asymptotic diffeomorphisms. These marginal modes can be viewed as the linearized precursors of BMS supertranslations, encoding conserved charges at spatial infinity.

**Remark 8** (Spectral interpretation of asymptotic symmetry). *The appearance of an extended zero mode at the inverse-cube threshold signals the enlargement of the asymptotic symmetry algebra to include nontrivial diffeomorphisms acting at infinity. The spectral transition at  $p = 3$  thus links the mathematical onset of noncompactness to the physical emergence of memory and soft graviton behavior within a common framework.*

**Universality of the spectral threshold.** The coincidence of analytic, numerical, and geometric evidence suggests that the inverse-cube decay represents a universal spectral boundary for long-range field theories on  $\mathbb{R}^3$ . In both gauge and gravitational contexts, curvature or field strength decaying as  $r^{-3}$  marks the transition between compact and noncompact spectral behavior, where the Laplacian ceases to dominate the asymptotic dynamics. This threshold thus defines a geometric law of infrared structure: it separates the radiative regime, characterized by freely propagating modes, from the marginal regime in which curvature produces algebraic tails and soft correlations that persist to infinity.

## 7 Relation to Previous Work and Threshold Phenomena

The spectral threshold established in Sections 3-5 connects several independent developments in spectral geometry, mathematical relativity, and gauge theory. It refines classical results on elliptic operators on asymptotically flat manifolds, relates to long-range scattering and tail phenomena in black-hole perturbation theory, and parallels curvature-controlled infrared thresholds first identified in non-Abelian gauge theory.

### 7.1 Spectral theory of elliptic operators on asymptotically flat ends

The analytic foundation for elliptic operators on noncompact manifolds with Euclidean ends was laid by Lockhart and McOwen [12]. They proved Fredholm and isomorphism properties for elliptic operators acting between weighted Sobolev spaces  $H_\delta^2 \rightarrow L_{\delta-2}^2$ , identifying indicial roots as the precise obstructions to invertibility. These results underlie much of geometric analysis on asymptotically flat manifolds, including the constraint equations of general relativity and deformation theory of vacuum initial data.

**Remark 9** (Extension of classical elliptic results). *Earlier analyses treated curvature terms as short-range perturbations of the Laplacian without identifying a quantitative boundary between short- and long-range behavior. The present result provides a sharp criterion: if  $|\text{Riem}(x)| \leq C r^{-p}$  with  $p > 3$ , the curvature potential  $V_R$  is relatively compact with respect to  $\Delta_T$  and*

$\sigma_{\text{ess}}(L) = [0, \infty)$ ; when  $p = 3$ , compactness fails and a normalized Weyl sequence appears at zero energy. This refines the Lockhart-McOwen framework by isolating the exact curvature decay rate at which the Fredholm property transitions to noncompact spectral behavior.

## 7.2 Thresholds in long-range potentials

The  $r^{-3}$  boundary identified here is the tensorial analogue of the classical long-range threshold in Schrödinger theory. In three dimensions, Simon [1] proved that potentials decaying faster than  $r^{-3}$  yield purely absolutely continuous spectrum on  $[0, \infty)$ , whereas slower decay allows resonances or threshold states near zero energy. The gravitational case exhibits an analogous structure, with the Riemann curvature playing the role of an effective potential.

**Remark 10** (Connection with Schrödinger thresholds). *The Lichnerowicz operator realizes, at the tensorial level, the same balance between dispersion and long-range coupling that governs Schrödinger operators. The inverse-cube decay marks the onset of marginally extended configurations, beyond which curvature ceases to influence the spectrum. This correspondence illustrates the structural similarity of infrared thresholds across scalar, vector, and tensor field equations.*

## 7.3 Relation to late-time tails in black-hole spacetimes

Price [13] and Ching *et al.* [11] showed that perturbations of the Schwarzschild spacetime decay as  $t^{-2\ell-3}$ , with the algebraic tail arising from an effective potential proportional to  $r^{-3}$ . The same scaling controls the marginal behavior of the spatial Lichnerowicz operator.

**Remark 11** (Spatial origin of temporal tails). *The elliptic analysis here provides the stationary counterpart of the dynamical late-time decay law. At the inverse-cube decay, the spatial operator supports near-zero modes that correspond to the low-frequency enhancement responsible for algebraic relaxation. The threshold  $p = 3$  thus unifies the stationary and dynamical manifestations of gravitational infrared behavior.*

## 7.4 Infrared structure and memory

In the context of asymptotic symmetry and gravitational memory, zero-frequency perturbations encode residual deformations between radiative vacua at null infinity. The existence of an  $L^2$ -normalized Weyl sequence at zero energy provides a spatial realization of these soft configurations.

**Remark 12** (Spectral characterization of the infrared sector). *At curvature decay  $|\text{Riem}| \sim r^{-3}$ , the Lichnerowicz operator develops marginally extended tensor modes that remain spatially nonlocal yet finite in energy. These represent the elliptic, spatial manifestation of soft graviton modes and delineate the precise geometric condition for the emergence of an infrared sector in linearized gravity.*

## 7.5 Parallel thresholds across gauge and gravitational systems

A closely related threshold occurs in non-Abelian gauge theory. For the covariant Laplacian

$$\Delta_A = -(\nabla_A)^* \nabla_A = -\nabla^* \nabla + \text{ad}(F_A),$$

acting on adjoint-valued fields with curvature  $F_A$ , the decay  $|F_A| \sim r^{-3}$  separates spectrally radiative behavior from the onset of infrared sensitivity.

**Proposition 2** (Parallel inverse-cube threshold). *For Laplace-type operators on bundles over  $\mathbb{R}^3$ , a curvature decay of order  $r^{-3}$  marks the transition between short-range, radiative behavior and long-range, infrared coupling. In both gauge and gravitational settings, curvature acts as an effective potential; at this critical rate, marginal nonlocalized modes appear, signaling the breakdown of compactness of the resolvent.*

## 7.6 Summary and outlook

Taken together, these results connect several domains of spectral analysis and physical theory. For  $p > 3$ , curvature perturbations are short-range and the spectrum purely radiative. At  $p = 3$ , curvature ceases to be compact, marginal modes emerge, and the infrared sector appears continuously but sharply. For  $p < 3$ , curvature strengthens the coupling further, but without forming discrete bound states in the present tensorial setting.

**Remark 13** (Open directions). *Future work should establish a full limiting absorption principle at the critical rate and extend the analysis to coupled gravity–gauge systems. Such results would provide a rigorous foundation for the infrared correspondence between soft sectors, asymptotic symmetries, and spectral transitions.*

## 8 Conclusion

The analyses presented here establish a sharp spectral threshold for the spatial Lichnerowicz operator on asymptotically flat three–manifolds. The results integrate geometric analysis, spectral theory, and physical interpretation within a unified framework.

**Theorem 2** (Spectral threshold for linearized gravity). *Let  $(\Sigma, g)$  be a smooth asymptotically flat three–manifold with curvature decay  $|\text{Riem}(x)| \leq C r^{-p}$ . Then:*

1. *For  $p > 3$ , the curvature potential  $V_R$  is relatively compact with respect to  $\nabla^* \nabla$ , and the essential spectrum is purely continuous:*

$$\sigma_{\text{ess}}(L) = [0, \infty).$$

2. *At the critical rate  $p = 3$ , compactness fails and a normalized Weyl sequence appears at zero energy, producing marginally extended tensor configurations that remain spatially nonlocal yet finite in energy.*
3. *For  $p < 3$ , curvature acts as a long-range potential that enhances infrared coupling, but without producing isolated bound states in the tensorial sector.*

**Remark 14** (Physical regimes). *The three regimes delineated above correspond respectively to radiative propagation ( $p > 3$ ), marginal persistence ( $p = 3$ ), and enhanced infrared coupling ( $p < 3$ ). The inverse–cube decay therefore represents the sharp geometric boundary between short-range and long-range gravitational behavior in three spatial dimensions.*

These findings extend classical spectral theory to curvature–coupled tensor operators and reveal a structural parallel with non–Abelian gauge fields and Schrödinger operators. In all three settings, the inverse–cube decay

marks the point at which the potential ceases to be spectrally negligible and marginal modes first appear. Numerical analysis of the reduced model confirms that this transition occurs continuously but sharply at  $p = 3$ , with no evidence of discrete confinement, validating the analytic predictions of Sections 3-5.

**Remark 15** (Future directions). *Several open problems arise naturally from this work: establishing a limiting absorption principle at the critical rate; extending the spectral analysis to Schwarzschild and Kerr slices; and developing the full dynamical correspondence between marginal spatial modes and the soft-memory sector at null infinity. Such results would further clarify the geometric and spectral unity of the infrared structure in gauge and gravitational theories.*

## Declarations

**Funding** The author received no external funding.

**Conflict of interest** The author declares no conflict of interest.

**Data availability** All data supporting the conclusions of this work are contained within the article and its Supplementary Material. No external datasets were used. Numerical results can be reproduced using the procedures described in Section 5 and Appendix D.

## A Gauge Correction and Elliptic Estimates

This appendix justifies the harmonic-gauge correction used in Section 3. Under the hypotheses of Section 5, namely,  $(\Sigma, g)$  smooth, asymptotically flat, simply connected, and with  $\text{Ric} = O(r^{-3})$ , the vector Laplacian

$$\Delta_V X = \nabla^* \nabla X + \text{Ric}(X)$$

is uniformly elliptic and symmetric on  $L^2(\Sigma; T^*\Sigma)$ .

**Lemma 4** (Isomorphism property). *For weights  $-1 < \delta < 0$ , the mapping*

$$\Delta_V : H_\delta^2(\Sigma; T^*\Sigma) \rightarrow L_{\delta-2}^2(\Sigma; T^*\Sigma)$$

*is Fredholm of index zero and an isomorphism whenever  $H_{\text{dR}}^1(\Sigma) = 0$ .*

*Sketch.* A direct consequence of Lockhart-McOwen theory (*Comm. Pure Appl. Math.* **38**, 603 (1985)), since the Euclidean indicial roots are  $\{0, -2\}$ .  $\square$

**Lemma 5** (Gauge correction). *For each  $h \in H_\delta^2(\Sigma; S^2 T^* \Sigma)$  with  $-1 < \delta < 0$ , there exists a unique  $X \in H_\delta^2(\Sigma; T^* \Sigma)$  satisfying  $\Delta_V X = \nabla \cdot h$  and  $\|X\|_{H_\delta^2} \leq C \|\nabla \cdot h\|_{L_{\delta-2}^2}$ .*

**Proposition 3** (Corrected Weyl sequence). *Let  $\{h_n\}$  be the approximate sequence of Section 3. Defining  $\tilde{h}_n = h_n - \mathcal{L}_{X_n} g$  with  $X_n = \Delta_V^{-1}(\nabla \cdot h_n)$  yields*

$$\|\tilde{h}_n\|_{L^2} = 1, \quad \tilde{h}_n \rightharpoonup 0, \quad \|L\tilde{h}_n\|_{L^2} \rightarrow 0.$$

*Thus  $0 \in \sigma_{\text{ess}}(L)$  in harmonic gauge.*

## B Curvature Structure and the Schwarzschild Example

The Schwarzschild metric provides a physical realization of the critical inverse-cube curvature decay analyzed in Section 3.

**Definition 2** (Spatial metric). *In isotropic coordinates  $(t, r, \omega)$ , the Schwarzschild line element is*

$$ds^2 = -\left(\frac{1 - \frac{M}{2r}}{1 + \frac{M}{2r}}\right)^2 dt^2 + \left(1 + \frac{M}{2r}\right)^4 (dr^2 + r^2 d\omega^2).$$

*On a time-symmetric slice  $t = \text{const.}$ , the spatial metric is  $g_{ij} = \psi^4 \delta_{ij}$  with  $\psi(r) = 1 + \frac{M}{2r}$ .*

**Lemma 6** (Asymptotic curvature). *For this metric,*

$$|\text{Riem}(x)| \simeq C M r^{-3} \quad (r \rightarrow \infty),$$

*so the curvature saturates the inverse-cube decay assumed in Theorem 2.*

**Proposition 4** (Effective potential). *The spatial Lichnerowicz operator on the Schwarzschild background satisfies*

$$Lh = \Delta_0 h - (CM)r^{-3}h + O(r^{-4})h, \quad CM > 0,$$

showing that the Schwarzschild geometry realizes, in its far-field limit, the same attractive  $r^{-3}$  potential analyzed in the numerical model of Section 5. <sup>4</sup>

## C Analytical Framework and Weighted Sobolev Spaces

We summarize the analytic conventions and functional-analytic tools used throughout.

**Definition 3** (Weighted Sobolev spaces). *For a smooth radius function  $r$  on an asymptotically flat three-manifold  $(\Sigma, g)$  and  $\delta \in \mathbb{R}$ ,*

$$\|u\|_{H_\delta^k}^2 = \sum_{|\alpha| \leq k} \int_{\Sigma} (1 + r^2)^{\delta - |\alpha|} |\nabla^\alpha u|^2 dV_g.$$

*Then  $H_\delta^k(\Sigma; E)$  is the completion of  $C_c^\infty(\Sigma; E)$  under this norm.*

**Lemma 7** (Fredholm property). *If  $P$  is a uniformly elliptic operator approaching constant coefficients at infinity, then*

$$P : H_\delta^2 \rightarrow L_{\delta-2}^2$$

*is Fredholm for all  $\delta$  not equal to an indicial root [12].*

**Proposition 5** (Self-adjointness and essential spectrum). *For  $\delta \in (-1, 0)$  and  $V = O(r^{-p})$  with  $p > 2$ , operators of the form  $L = \nabla^* \nabla + V$  are self-adjoint on  $L^2(\Sigma; E)$ . The essential spectrum  $\sigma_{\text{ess}}(L)$  is determined by the existence of Weyl sequences as in Weyl's criterion.*

**Lemma 8** (Compactness of the curvature potential for  $p > 3$ ). *Let  $(\Sigma, g)$  be a smooth asymptotically flat three-manifold with a single Euclidean end, and assume*

$$g_{ij} = \delta_{ij} + O(r^{-1}), \quad \partial g_{ij} = O(r^{-2}), \quad \partial^2 g_{ij} = O(r^{-3}),$$

*so that  $|\text{Riem}(x)| \leq C \langle r \rangle^{-p}$  for some  $p > 3$ . Fix a weight  $-1 < \delta < 0$ , and let*

$$L = \nabla^* \nabla + V_R, \quad (V_R h)_{ij} = -R_i^{\ell}{}_j{}^m h_{\ell m}.$$

---

<sup>4</sup>The overall minus sign arises from the definition  $(V_R h)_{ij} = -R_i^{\ell}{}_j{}^m h_{\ell m}$ , which makes the curvature coupling attractive for positive mass  $M > 0$ .

Then the curvature term defines a compact operator

$$V_R : H_\delta^2(\Sigma; S^2 T^* \Sigma) \longrightarrow L_{\delta-2}^2(\Sigma; S^2 T^* \Sigma),$$

and therefore  $L$  is a compact perturbation of  $\nabla^* \nabla$  on  $L^2(\Sigma; S^2 T^* \Sigma)$ . In particular,

$$\sigma_{\text{ess}}(L) = \sigma_{\text{ess}}(\nabla^* \nabla) = [0, \infty).$$

*Proof.* The curvature bound  $|\text{Riem}(x)| \leq C \langle r \rangle^{-p}$  implies  $|V_R(x)| \leq C \langle r \rangle^{-p}$ , so that for any  $h \in H_\delta^2(\Sigma; S^2 T^* \Sigma)$ ,

$$\|V_R h\|_{L_{\delta-2}^2}^2 = \int_{\Sigma} \langle r \rangle^{2(\delta-2)} |V_R(x)h(x)|^2 dV_g \lesssim \int_{\Sigma} \langle r \rangle^{2(\delta-2)-2p} |h(x)|^2 dV_g.$$

Since  $-1 < \delta < 0$  and  $p > 3$ , the exponent  $2(\delta - 2) - 2p$  is less than  $-6$ , making the weight  $\langle r \rangle^{2(\delta-2)-2p}$  integrable at infinity in three dimensions. Hence  $V_R : H_\delta^2 \rightarrow L_{\delta-2}^2$  is bounded.

To verify compactness, let  $\chi_R$  be a smooth cutoff equal to 1 on  $\{r \leq R\}$  and supported in  $\{r \leq 2R\}$ . Decompose

$$V_R = \chi_R V_R + (1 - \chi_R) V_R =: V_R^{(\text{comp})} + V_R^{(\text{tail})}.$$

On the bounded region  $\{r \leq 2R\}$ , the metric is smooth and the weighted norms are equivalent to the unweighted ones. By the classical Rellich compactness theorem on precompact domains, the embedding  $H_\delta^2(\{r \leq 2R\}) \hookrightarrow L_{\delta-2}^2(\{r \leq 2R\})$  is compact; since  $V_R$  is smooth there, the multiplication operator  $V_R^{(\text{comp})}$  is compact.

The remainder  $V_R^{(\text{tail})}$  is supported in  $\{r > R\}$ , where the curvature decay dominates. For  $h$  with  $\|h\|_{H_\delta^2} = 1$ ,

$$\|V_R^{(\text{tail})} h\|_{L_{\delta-2}^2}^2 \lesssim \int_{r>R} \langle r \rangle^{2(\delta-2)-2p} |h(x)|^2 dV_g.$$

Because  $2(\delta - 2) - 2p < -6$ , the weight decays faster than  $r^{-6}$ ; combined with the uniform bound  $|h|^2 \in L_\delta^2$ , dominated convergence implies that

$$\sup_{\|h\|_{H_\delta^2}=1} \|V_R^{(\text{tail})} h\|_{L_{\delta-2}^2} \longrightarrow 0 \quad \text{as } R \rightarrow \infty.$$

Thus  $V_R$  is the limit of compact operators with vanishing tails, and hence compact.

Finally, since  $L = \nabla^* \nabla + V_R$  is a compact perturbation of the nonnegative, self-adjoint operator  $\nabla^* \nabla$ , Weyl's theorem ensures that the essential spectra coincide:

$$\sigma_{\text{ess}}(L) = \sigma_{\text{ess}}(\nabla^* \nabla) = [0, \infty).$$

The essential spectrum of the Lichnerowicz operator therefore matches that of the flat tensor Laplacian, confirming that sufficiently rapid curvature decay leaves the asymptotic spectrum purely continuous.  $\square$

**Remark 16.** *These weighted spaces and mapping properties justify the estimates and compactness arguments used in Sections 2–3.*

## D Numerical Validation and Stability Tests

This appendix documents three numerical consistency checks supporting the eigenvalue results reported in Section 5: (i) grid-spacing convergence, (ii) finite-volume convergence in  $R_{\max}$ , and (iii) robustness under constraint enforcement. These tests show that the observed spectral transition near  $p = 3$  is not a numerical artifact of discretization, boundary conditions, or gauge penalties.

### D.1 Grid refinement at fixed physical volume

To verify that the numerical results reported in Section 5 are free from discretization artifacts, we repeated the computations at two grid resolutions. The coarse run used spacing  $h \approx 1.0$  ( $N = 21$  points per axis,  $\sim 4.1 \times 10^4$  degrees of freedom), and the refined run used  $h \approx 0.5$  ( $N = 41$ ,  $\sim 3.6 \times 10^5$  degrees of freedom). Converged eigenvalues at both resolutions are listed below. The near-invariance of  $\lambda_1$  and  $\lambda_2$  confirms that the numerical spectrum is stable with respect to grid refinement and that the observed scaling behavior in Section 5 is not a numerical artifact.

*Coarse resolution ( $h \approx 1.0$ ,  $N = 21$  points/axis,  $\sim 4.1 \times 10^4$  DOFs).*

$$\begin{aligned} \text{flat: } \quad \lambda_1 &= 0.07386996, & \lambda_2 &= 0.14713361, \\ p = 2.5 : \quad \lambda_1 &= 0.06505331, & \lambda_2 &= 0.07023744, \\ p = 3.0 : \quad \lambda_1 &= 0.07114971, & \lambda_2 &= 0.07276003, \\ p = 3.5 : \quad \lambda_1 &= 0.07298806, & \lambda_2 &= 0.07351824. \end{aligned}$$

Refined resolution ( $h \approx 0.5$ ,  $N = 41$  points/axis,  $\sim 3.6 \times 10^5$  DOFs).

$$\begin{aligned} \text{flat: } \quad \lambda_1 &= 0.07398399, \quad \lambda_2 = 0.14781594, \\ p = 2.5: \quad \lambda_1 &= 0.06505635, \quad \lambda_2 = 0.07029545, \\ p = 3.0: \quad \lambda_1 &= 0.07109678, \quad \lambda_2 = 0.07279109, \\ p = 3.5: \quad \lambda_1 &= 0.07295142, \quad \lambda_2 = 0.07355686. \end{aligned}$$

Halving the grid spacing changes  $\lambda_1$  by less than 0.2% across all  $p$ , demonstrating numerical convergence in  $h$ . Crucially, the ordering

$$\lambda_1(p=2.5) < \lambda_1(p=3.0) < \lambda_1(p=3.5) \simeq \lambda_1(\text{flat})$$

is preserved under refinement. This ordering encodes the physical trend reported in Section 5: slower curvature decay (smaller  $p$ ) produces a stronger infrared distortion of the lowest mode, while faster decay ( $p > 3$ ) becomes spectrally indistinguishable from flat space. The persistence of this structure under refinement shows that it is not a coarse-grid artifact.

## D.2 Finite-volume convergence in $R_{\max}$

We also varied the outer box size  $R_{\max} \in \{6, 10, 14, 18, 20\}$  at fixed grid spacing  $h \approx 1.0$  (so that increasing  $R_{\max}$  increases the number of unknowns) and observed that  $\lambda_1$  decreases monotonically with  $R_{\max}$  for every  $p$  tested. For example, at  $p = 3.0$  we find

$$\lambda_1(R_{\max}=6) = 0.1965, \quad \lambda_1(R_{\max}=10) = 0.0711, \quad \lambda_1(R_{\max}=20) = 0.0180.$$

The approximate scaling  $\lambda_1 \sim R_{\max}^{-2}$  agrees with the interpretation of  $\lambda_1$  as the lowest discrete ‘‘box mode’’ approaching the continuum threshold. This confirms that the small eigenvalues reported in Table 2 are controlled by the infrared volume scale and not spurious numerical locking to the boundary.

**Penalty strength studies and TT projection cross–check.** We sweep  $\eta, \zeta$  over two decades (e.g.  $\eta = \zeta \in \{10, 40, 160, 640\}$  in nondimensional units); for  $p \in \{2.5, 3.0, 3.5\}$  the relative shifts in  $\lambda_{1,2}$  between the two largest penalties are  $< 10^{-3}$ . We also compute the lowest eigenpair using an explicit TT projection: given any  $u$ , let  $u^{\text{TT}} = \Pi_{\text{TT}}u$  via Helmholtz–Hodge decomposition (solve  $\Delta_V X = \nabla \cdot u$ , then set  $u^{\text{TT}} = u - \mathcal{L}_X g - \frac{1}{3}(\text{tr } u)g$ ).

The projected–eigenpair agrees with the penalty result within the grid error. (Algorithmic details in Sec. S1; linear solves via conjugate gradients with algebraic multigrid preconditioner.)

**Remark 17** (Conclusion). *The convergence in grid spacing, the  $R_{\max}$  scaling, and the robustness under transverse-traceless enforcement all support a single interpretation: the trends reported in Section 5 reflect genuine infrared properties of the Lichnerowicz operator. In particular, they provide independent numerical evidence that the inverse-cube decay of curvature ( $p = 3$ ) marks the threshold between spectrally relevant long-range curvature and spectrally negligible curvature.*

**Code availability.** The complete Python script reproducing Table 2 is provided as `3d_tensor_operator.py` in the Supplementary Reproducibility Package (ResearchGate upload). It implements the finite-difference Laplacian, the regularized tidal curvature term  $E_{ij} \sim r^{-p}(n_i n_j - \delta_{ij}/3)$ , and the trace–penalty enforcement of the TT constraint.

## E Weyl Sequence Construction and Verification of the Critical Spectrum

This appendix provides quantitative estimates completing the proof of Lemma 2 and Theorem 1. Throughout,  $(\Sigma, g)$  satisfies the asymptotic flatness conditions of eq. 11 with  $|\text{Riem}(x)| \leq Cr^{-3}$ .

### Normalization and scaling

Let  $H_{ij}(\omega)$  be a trace-free, divergence-free harmonic on  $S^2$  and define  $h_n = A_n \phi_n(r) r^{-1} H_{ij}(\omega)$  with  $\phi_n$  supported on  $A_n = \{n/2 < r < 2n\}$ . The metric volume element satisfies  $dV_g = (1 + O(r^{-1}))r^2 dr d\omega$ , so that

$$\|h_n\|_{L^2}^2 \simeq A_n^2 \int_{n/2}^{2n} r^{-2} r^2 dr \sim A_n^2 n.$$

Choosing  $\|h_n\|_{L^2} = 1$  gives  $A_n \simeq n^{-1/2}$ . Derivatives of  $\phi_n$  are supported on the thin shells  $S_n = \{n/2 < r < n\} \cup \{3n/2 < r < 2n\}$  where  $|\nabla \phi_n| \lesssim n^{-1}$ .

## Commutator and curvature estimates

Expanding

$$\nabla^* \nabla (\phi_n r^{-1} H) = \phi_n \nabla^* \nabla (r^{-1} H) + 2 \nabla \phi_n \cdot \nabla (r^{-1} H) + (\Delta \phi_n) r^{-1} H,$$

the first term vanishes identically in flat space since  $\nabla^* \nabla (r^{-1} H) = 0$  for tensor harmonics of order  $\ell = 2$ . The commutator terms are supported on  $S_n$  and satisfy

$$\|[\nabla^* \nabla, \phi_n] h_n\|_{L^2} \lesssim n^{-2}.$$

The curvature potential obeys  $|V_R| \leq C r^{-3}$ , so that

$$\|V_R h_n\|_{L^2}^2 \lesssim A_n^2 \int_{n/2}^{2n} r^{-6} r^2 dr \sim n^{-4}, \quad \|V_R h_n\|_{L^2} \lesssim n^{-2}.$$

Together these give  $\|L h_n\|_{L^2} \lesssim n^{-2}$ .

## Gauge correction

Solving  $\Delta_V X_n = \nabla \cdot h_n$  with the Fredholm estimate of Lemma 1 yields

$$\|X_n\|_{H_\delta^2} \lesssim \|\nabla \cdot h_n\|_{L^2} \lesssim n^{-1}, \quad -1 < \delta < 0.$$

Hence  $\|\mathcal{L}_{X_n} g\|_{L^2} \lesssim n^{-1}$  and the corrected fields  $\tilde{h}_n = h_n - \mathcal{L}_{X_n} g$  satisfy  $\nabla^j \tilde{h}_{n,ij} = 0$ . Since  $L(\mathcal{L}_{X_n} g)$  involves at most two derivatives of  $X_n$ ,

$$\|L(\mathcal{L}_{X_n} g)\|_{L^2} \lesssim n^{-1},$$

which is subleading relative to  $\|L h_n\|_{L^2} \lesssim n^{-2}$ . Thus

$$\|L \tilde{h}_n\|_{L^2} \rightarrow 0, \quad \|\tilde{h}_n\|_{L^2} = 1.$$

## Conclusion

The sequence  $\{\tilde{h}_n\}$  is normalized, divergence-free, and supported on disjoint annuli escaping to infinity, implying  $\tilde{h}_n \rightharpoonup 0$  weakly in  $L^2$ . By Weyl's criterion,  $0 \in \sigma_{\text{ess}}(L)$ , establishing Theorem 1.

**Author contributions** The author is solely responsible for all aspects of this work.

## References

- [1] B. Simon, “On the genericity of nonvanishing of the low energy spectral density for Schrödinger operators,” *Ann. Phys. (N.Y.)* **97**, 279-288 (1976).
- [2] R. K. Sachs, “Gravitational waves in general relativity. VIII. Waves in asymptotically flat space-times,” *Proc. R. Soc. Lond. A* **270**, 103-126 (1962).
- [3] R. Bartnik, “The mass of an asymptotically flat manifold,” *Comm. Pure Appl. Math.* **39** (1986), no. 5, 661-693.
- [4] R. B. Lockhart and R. C. McOwen, “Elliptic differential operators on noncompact manifolds,” *Ann. Scuola Norm. Sup. Pisa Cl. Sci. (4)* **12**, 409-447 (1985).
- [5] H. Weyl, “Über gewöhnliche Differentialgleichungen mit Singularitäten und die zugehörigen Entwicklungen willkürlicher Funktionen,” *Math. Ann.* **68**, 220-269 (1910).
- [6] S. Agmon, *Lectures on Exponential Decay of Solutions of Second-Order Elliptic Equations*, (Princeton University Press, Princeton, 1982).
- [7] A. Ashtekar and M. Streubel, “Symplectic Geometry of Radiative Modes and Conserved Quantities at Null Infinity,” *Proc. R. Soc. Lond. A* **376**, 585-607 (1981).
- [8] H. Bondi, M. G. J. van der Burg and A. W. K. Metzner, “Gravitational waves in general relativity. VII. Waves from axisymmetric isolated systems,” *Proc. R. Soc. Lond. A* **269**, 21-52 (1962).
- [9] P. R. Chernoff, “Essential self-adjointness of powers of generators of hyperbolic equations,” *J. Funct. Anal.* **12**, 401-414 (1973).
- [10] D. Christodoulou, “Nonlinear nature of gravitation and gravitational-wave experiments,” *Phys. Rev. Lett.* **67**, 1486-1489 (1991).
- [11] E. S. C. Ching, P. T. Leung, W. M. Suen and K. Young, “Late-time tail of wave propagation on curved spacetime,” *Phys. Rev. Lett.* **74**, 4588-4590 (1995).

- [12] R. B. Lockhart and R. C. McOwen, “On elliptic systems in  $\mathbb{R}^n$ ,” *Acta Math.* **150**, 125-135 (1983).
- [13] R. H. Price, “Nonspherical perturbations of relativistic gravitational collapse. I. Scalar and gravitational perturbations,” *Phys. Rev. D* **5**, 2419-2438 (1972).
- [14] M. Reed and B. Simon, *Methods of Modern Mathematical Physics, Vol. IV: Analysis of Operators*, (Academic Press, New York, 1978).
- [15] T. Regge and J. A. Wheeler, “Stability of a Schwarzschild singularity,” *Phys. Rev.* **108**, 1063-1069 (1957).
- [16] A. Strominger, *Lectures on the Infrared Structure of Gravity and Gauge Theory*, (Princeton University Press, Princeton, 2018).
- [17] S. Weinberg, “Infrared photons and gravitons,” *Phys. Rev.* **140**, B516-B524 (1965).
- [18] M. Wilson, “Curvature Decay and the Spectrum of the Non-Abelian Laplacian on  $\mathbb{R}^3$ ”, ArXiv. <https://arxiv.org/abs/2511.03532> (2025), presented at the 2025 TAOAPS Conference. Submitted to the Journal of Spectral Theory.
- [19] Ya. B. Zel'dovich and A. G. Polnarev, “Radiation of gravitational waves by a cluster of superdense stars,” *Sov. Astron.* **18**, 17-23 (1974).
- [20] N. D. Birrell and P. C. W. Davies, *Quantum Fields in Curved Space* (Cambridge University Press, Cambridge, 1982).
- [21] R. M. Wald, *Quantum Field Theory in Curved Spacetime and Black Hole Thermodynamics* (University of Chicago Press, Chicago, 1994).
- [22] S. Chandrasekhar, *The Mathematical Theory of Black Holes* (Oxford University Press, Oxford, 1983).